Choice of saccade endpoint under risk

John F. Ackermann

Department of Psychology, New York University, New York, NY, USA

Michael S. Landy

Department of Psychology, New York University, New York, NY, USA
Department of Neural Science, New York University, New York, NY, USA

Eye movements function to bring detailed information onto the high-resolution region of the retina. Previous research has shown that human observers select fixation points that maximize information acquisition and minimize target location uncertainty. In this study, we ask whether human observers choose the saccade endpoint that maximizes gain when there are explicit rewards associated with correctly detecting the target. Observers performed an 8-alternative forced-choice detection task for a contrast-defined target in noise. After a single saccade, observers indicated the target location. Each potential target location had an associated reward that was known to the observer. In some conditions, the reward at one location was higher than at the other locations. We compared human saccade endpoints to those of an ideal observer that maximizes expected gain given the respective human observer's visibility map, i.e., d' for target detection as a function of retinal location. Varying the location of the highest reward had a significant effect on human observers' distribution of saccade endpoints. Both human and ideal observers show a high density of saccades made toward the highest rewarded and actual target locations. But humans' overall spatial distributions of saccade endpoints differed significantly from the ideal observer as they made a greater number of saccade to locations far from the highest rewarded and actual target locations. Suboptimal choice of saccade endpoint, possibly in combination with suboptimal integration of information across saccades, had a significant effect on human observers' ability to correctly detect the target and maximize gain.

Introduction

We move our eyes in the process of gathering information. The visible aspects of an object give us information regarding its presence, location, size, shape, and identity, among other things. But for a foveated visual system, detailed information is not available in the far periphery of the visual field. For fine detail to be visible, we must shift our gaze so that the image falls on the high-resolution fovea.

In many cases, the value of the information at some locations is greater than at others. A pilot, for example, has information coming from both the instrument panel in the lower visual field and from outside of the windshield in the upper visual field. When flying in fog, the view outside the windshield has little value and the pilot benefits most from shifting gaze to the instrument panel. On the other hand, when coming in for a landing on a clear day, the view outside the windshield may have more to offer. This type of situation has been likened to foraging for information (Herrnstein, 1970; Sugrue, Corrado, & Newsome, 2004). People tend to select fixation locations with the highest value (Bisley & Goldberg, 2010).

How good are we at selecting the fixation position that gives the greatest possible benefit? Najemnik and Geisler (2005) asked observers to search for a Gabor target embedded in a 15° diameter field of $1/f$ noise. They found that the number of saccades and distribution of saccade endpoints were consistent with the predictions of an optimal observer that chooses each endpoint so as to reduce target-location uncertainty.

Similar results were found by Renninger, Verghese, and Coughlan (2007). Observers had 1.2 s to learn an abstract shape presented visually. They were subsequently presented with two such shapes and asked to indicate which was the previously learned shape. Observers tended to make three to five saccades during the learning phase. The distribution of saccade endpoints was best predicted by a model that selects maximum-entropy regions, i.e., regions along the edge of the shape in which orientation varies maximally, and

Citation: Ackermann, J. F., & Landy, M. S. (2013). Choice of saccade endpoint under risk. *Journal of Vision*, *13*(3):27, 1–20, http://www.journalofvision.org/content/13/3/27, doi:10.1167/13.3.27.

doi: 10.1167/13.3.27 Received July 3, 2012; published September 10, 2013 ISSN 1534-7362

which thereby offer the most information about the shape.

Both of these results suggest that human observers choose the saccade endpoint that gives them the most information for the current task. That is, it appears that observers maximize the information gained per saccade, thus treating "information" as a form of reward. But, does saccade behavior change in the presence of concrete monetary rewards? Navalpakkam, Koch, Rangel, and Perona (2010) presented subjects with eight oriented line stimuli arranged along the circumference of an invisible circle. Two of these, one horizontal and one vertical line, were search targets. The remaining six were oblique distracters. Subjects received monetary rewards for identifying a target location. Observers' choices were best explained by a model that maximizes expected reward by calculating the probability of a target occurring at each location, multiplying each probability by its respective reward (i.e., computing the expected gain for choosing that location) and choosing the location that would lead to maximum expected gain. However, in this task, the observer's choice of target location was made based on exposure to the stimulus at the initial fixation location only; the stimulus was too brief for observers to make a saccade.

In the study reported here, observers searched for a target in an array in which there was a prespecified reward for correct detection of a target at each location. We asked whether observers optimally chose the location for the saccade that preceded their decision as a function of reward condition. We compared human observers' choice of fixation, performance in detecting the target, and their monetary gain with that of an ideal observer that maximizes expected gain. Human observers' choice of fixation and detection performance differed significantly from that of the ideal observer. Human observers' monetary gain never fell far below the ideal observer's. However, we show that human observers' gain is not greater than that of a searcher that chooses a saccade endpoint randomly on each trial. This suggests that the cost to the human observers in unobtained rewards is potentially substantial, depending on the specific reward structure of the task.

Methods

Observers

Four subjects (one female), including the author (JFA), participated for compensation in the amount of $10 per session for nine sessions, in addition to a performance-based reward, described below, which ranged from $68 to $90 across subjects. Subjects signed a consent form approved by the New York University University Committee on Activities Involving Human Subjects.

Apparatus

Stimuli were presented on a gamma corrected, 36 × 27 cm, Sony Multiscan G400 monitor with a resolution of 1600 × 1200 pixels, a refresh rate of 75 Hz, and a mean luminance of 40 cd/m^2. Eye position was monitored using an SR Research Eyelink1000 tower-mount eye tracker with a sampling rate of 1000 Hz, controlled using the Eyelink Toolbox Matlab interface (Cornelissen, Peters, & Palmer, 2002).

Stimuli and procedure

The target stimulus in all conditions consisted of a 2° diameter, 3 cycle/deg Gabor patch in cosine phase (Gaussian envelope $SD = 0.66°$), masked by additive Gaussian white noise covering the same 2° diameter patch. Mean luminance was 40 cd/m^2. Signal contrast was at most 50%. Noise SD was 16.7% contrast, and noise values were clipped at three SDs above and below the mean, so that luminance values always lay within the display gamut. The observer sat at a distance of 42 cm from the monitor. Head position was constrained by a chin rest firmly attached to the eye tracker. Each block of trials began with a nine-point spatial calibration of the eye tracker.

Preliminary experiment

The first step was to derive a map for each observer giving the detectability of the search target for all locations across the visual field. Each observer's visibility map was used subsequently to model the behavior of an ideal observer.

The trial sequence is shown in Figure 1A. Each trial began with a white fixation cross (0.33° × 0.33°) at the center of the screen on a gray, mean-luminance background. Detectability was measured at 25 locations at 0°, 4°, 8°, and 12° eccentricity and polar positions at multiples of 45° (Figure 1B). At the beginning of each trial a 2° diameter white ring appeared to indicate which of the 25 locations, selected at random, was the target for that trial. On trials in which the target appeared at the center of the screen, the ring replaced the fixation cross. The observer fixated the cross (or ring) and initiated the stimulus presentation by key press. The observer was signaled to

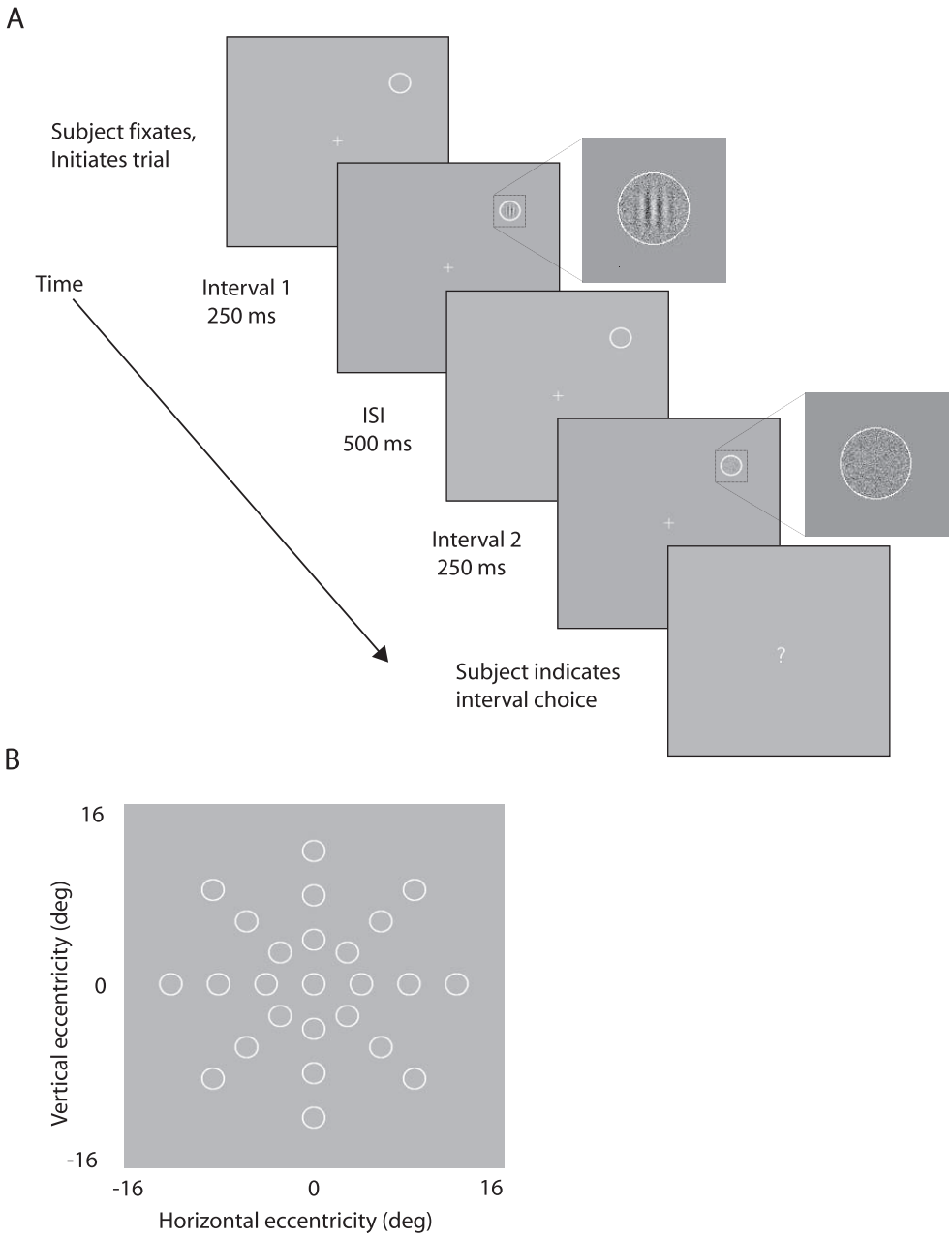

Figure 1. (A) Trial sequence for the preliminary experiment with example target and noise stimuli shown in Intervals 1 and 2, respectively (target contrast is exaggerated for display purposes). (B) Target positions in the preliminary experiment.

reattempt initiation of the trial if current eye position was more than 1° away from the center of the cross.

The observer's task was to indicate which of two 250 ms temporal intervals, separated by a 500 ms interstimulus interval, contained the target (two-interval forced choice, 2IFC). The nontarget interval contained noise alone. Gabor contrast was varied using two interleaved staircases (one-up/two-down, one-up/three-down) for each stimulus location (Treutwein, 1995). Trials in which eye position shifted more than 1° from fixation before the end of the second interval were terminated and repeated at random later in the block. At the end of the second interval, the fixation cross was replaced by a question mark signaling the observer to indicate the target interval by key press.

Two staircases of 100 trials each were run for each of the 25 stimulus locations, for a total of 5,000 trials. These trials were completed over five sessions of 1,000 trials each on separate days, with staircases continuing across the five sessions.

The visibility map describes the probability of responding correctly in the 2IFC task in response to a stimulus of contrast c at retinal location r, θ (in polar coordinates relative to the fovea). We assume a Weibull

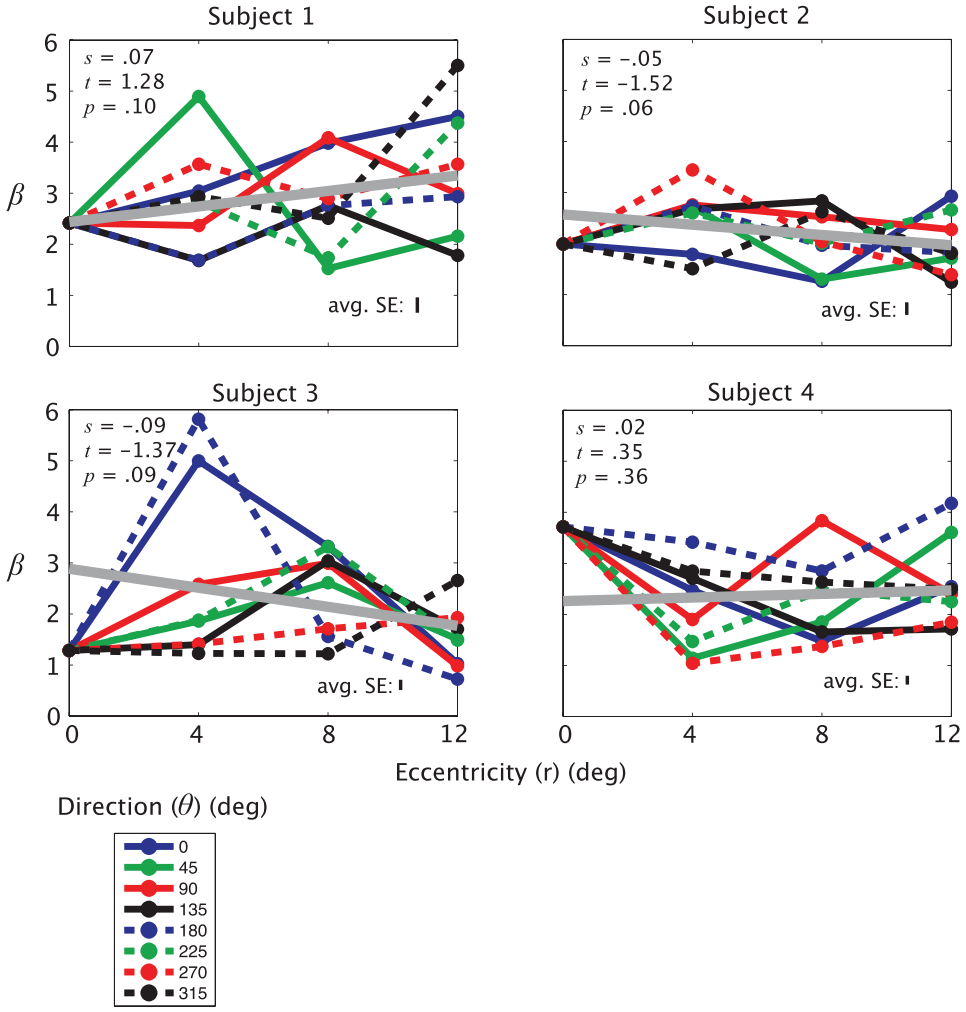

Figure 2. The fit steepness parameters, β, for Weibull functions fit to each of the 25 locations tested in the preliminary experiment, as a function of eccentricity (r) and direction (θ). Error bars show the *SE* of the β values averaged across the 25 locations as determined by bootstrapping. For each subject, the best fitting regression line is shown in gray with the regression slope, *s*, *t* value of the test for a significant difference between the slope and zero, and the resulting *p* value. No slopes are significantly different from zero and thus we assume a constant steepness parameter for the visibility-map fits.

psychometric function

$$p(r,\theta) = 1 - .5e^{-(c/\alpha(r,\theta))^{\beta}}, \quad (1)$$

where p is the probability of a correct response. Several studies have shown that the steepness parameter, β, changes as a function of eccentricity (Geisler, Perry, & Najemnik, 2006; Michel & Geisler, 2011; Najemnik & Geisler, 2005). To determine the effect of both eccentricity (r) and direction (θ) on β, we fit Weibull psychometric functions independently to the data for each of the 25 stimulus locations (each with a single threshold parameter α and steepness parameter β). We regressed, for each subject, the fit βs onto r and θ. Regression slopes were not significantly different from zero. The fit βs are shown in Figure 2 with the results of the regression of β onto eccentricity. The steepness parameters did not vary systematically with eccentricity or direction. Therefore, we treat β in Equation 1 as constant across the visual field.

Thresholds were assumed to be jointly dependent on eccentricity and polar angle with the form

$$\alpha(r,\theta) = a_1 + a_2 e^{g(\theta)r}, \quad (2)$$

where

$$g(\theta) = a_3\Big(1 + a_4 \sin(\theta + a_5) + a_6 \sin(2\theta + a_7)\Big). \quad (3)$$

The a_i and β are parameters fit to the data. The $\sin\theta$ term allows g to account for the vertical meridian asymmetry in which stimuli are more detectable at the bottom than at the top of the visual field (Liu, Heeger, & Carrasco, 2006; Previc, 1990). The $\sin 2\theta$ term allows for the vertical/horizontal asymmetry in which stimuli are

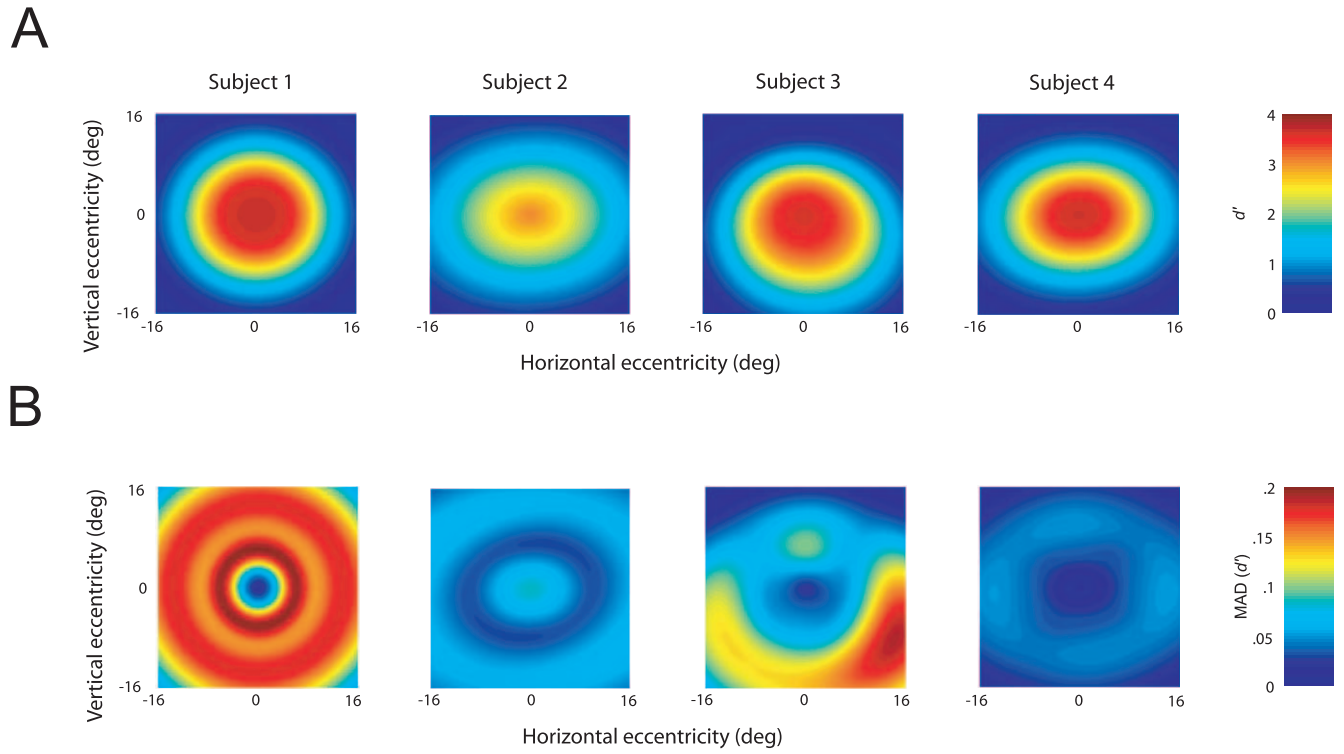

Figure 3. (A) Detectability (d') as a function of retinal location for each subject. Each map represents detectability for the stimulus contrast used in the main experiment: Michelson contrast = 16%. (B) The median absolute deviation (MAD) of each map's d' estimates as determined by bootstrapping (see text).

more detectable along the horizontal than the vertical meridian (Carrasco, Talgar, & Cameron, 2001). The exponential form allowed α to model the increase of threshold in the periphery. p values from Equation 1 were converted to d' (Wickens, 2002):

$$d' = \sqrt{2}\Phi^{-1}(p), \quad (4)$$

where Φ^{-1} is the inverse of the cumulative standard normal distribution. Visibility maps for each subject are shown in Figure 3A for detectability at the stimulus contrast used in the main experiment: Michelson contrast = 16%.

To calculate the error associated with each visibility map, we fit the above Weibull function to 1,000 bootstrapped iterations (Efron & Tibshirani, 1993) of the experiment given each subject's data (and assuming, as before, a single steepness parameter β across locations). We determined the magnitude of the error by calculating the median absolute deviation of d', for a signal contrast of 16%, as a function of eccentricity across the 1,000 fits for each subject. The result is shown in Figure 3B. We also calculated the signed deviations of the bootstrapped fits from the empirically measured visibility maps (Figure 3A) by taking the median of the difference between the bootstrapped d' values and the d' value of the visibility map at each horizontal and vertical coordinate. The signed error of the fits does not show a consistent spatial pattern across subjects and the median absolute deviations of the fit (Figure 3B) are relatively small, suggesting that our model of the detectability map will suffice for guiding our ideal observer.

Main experiment

In the main experiment, subjects performed a visual search task in which the reward for correct detection varied across potential target locations and saccade endpoints were measured. We were interested in the strategy for choice of saccade endpoint. The greater the number of saccades, the less the observer stands to lose for a single, poorly chosen saccade endpoint. Thus, we allowed subjects only a single saccade prior to indicating the location of the target. The trial sequence is shown in Figure 4A. Each trial began with a fixation cross at the center of the screen and eight 2° diameter rings placed at 45° intervals along the circumference of an invisible 12° diameter circle. Each ring contained Gaussian white noise. Adjacent to each ring was a number indicating the reward in points for correctly detecting the target should it appear within that ring.

There were five reward conditions (Figure 4B). In one (equal rewards) condition, the values of a correct response were 100 points for each of the eight target locations. In the other four (unequal rewards) condi-

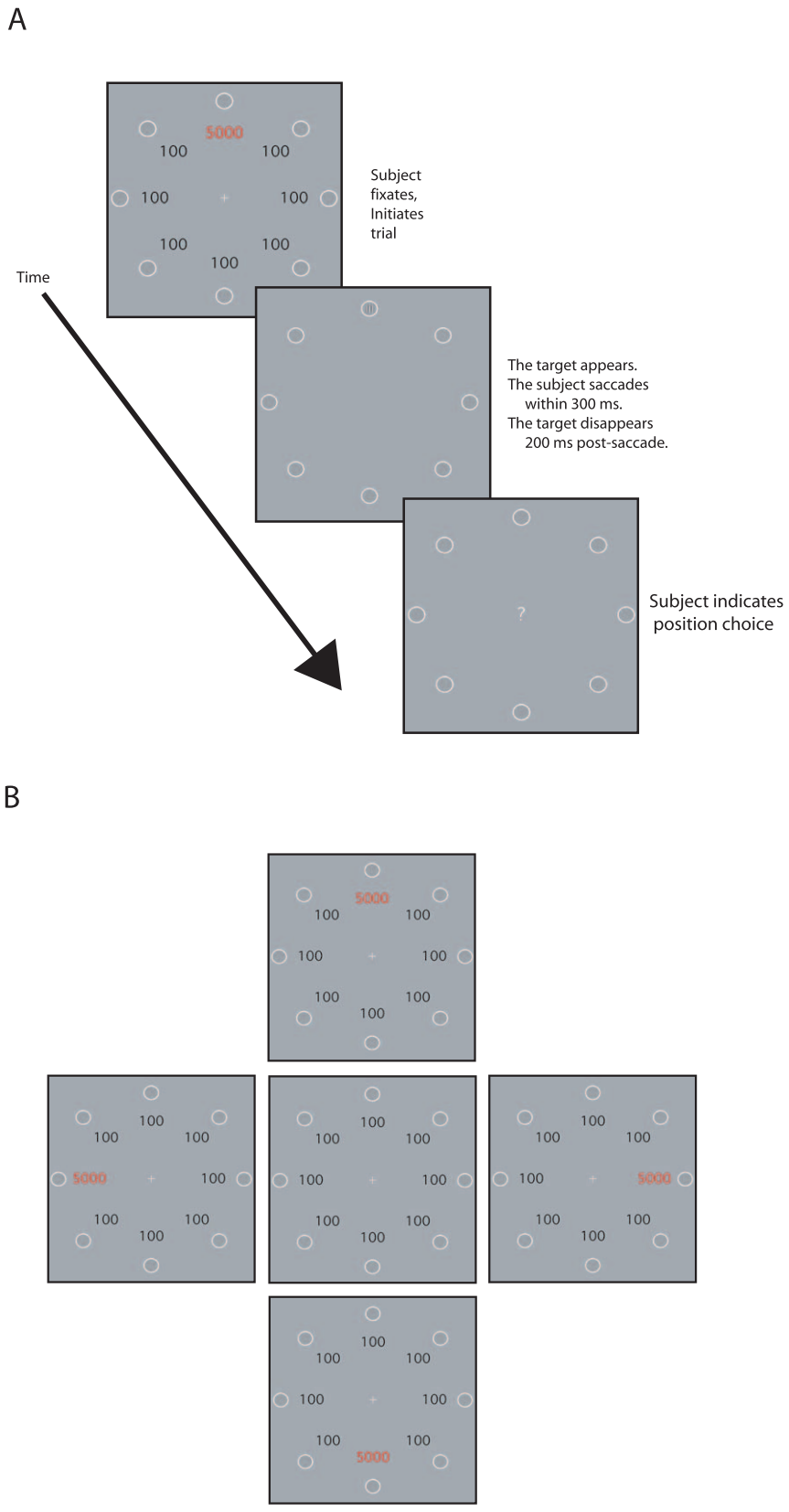

Figure 4. (A) Trial sequence for the main experiment. (B) The five reward conditions for the main experiment.

tions, the value of one location was always 5,000 points and the other seven locations, 100 points. The location of the highest reward was varied as shown. The reward condition was chosen at random on every trial. Varying the highest rewarded location in this way should lead to a systematic bias in the choice of saccade endpoint (Liston & Stone, 2008).

The observer fixated the cross and initiated stimulus presentation by key press. A 16%-contrast target was then added to one of the eight rings chosen at random. The observer was required to initiate a saccade within 300 ms of stimulus appearance (i.e., after the key press). Saccade initiation and termination were detected using the Eyelink 1000's online parser. Saccade initiation was signaled when eye position deviated more than 2° from initial fixation, velocity exceeded 30°/sec, and acceleration exceeded 8000°/sec^2. A saccade was deemed complete when either velocity or acceleration fell below threshold. The ideal-observer model we use requires pre- and post-saccadic noise to be uncorrelated. Thus, once saccade initiation was detected, new random noise fields were displayed in each ring. The target was displayed for 200 ms following termination of the saccade, so that subjects were prevented from gaining target information by making additional eye movements. When the target disappeared, leaving the eight noise fields, a question mark appeared at the center of the screen. The observer indicated the target position by fixating the corresponding ring.

The ideal-observer model we develop below hypothesizes that subjects choose the saccade endpoint that maximizes the expected gain (EG) of the choice of target position that follows the saccade. The model computes EG for all possible saccade endpoints, and the predictions are strongest if the EG map has a well-defined peak. We simulated ideal-observer-model performance for a range of stimulus contrasts and target eccentricities, using each observer's visibility map, and derived an EG map for one simulated trial for each of the 40 (5 Reward × 8 Target Location) conditions. The EG map always has a single peak value at one spatial location due to the structure of the visibility maps: Visibility is always maximal at fixation. When stimulus contrast is high, the EG map is relatively flat, with only a nominal peak, because the target is already identifiable from the initial fixation. When stimulus contrast is low or the target is peripheral, the initial fixation yields little information about target position, and again the EG map is flat. To ensure that the peak of the EG map is, on average, substantially greater than the nonpeak regions, we calculated the proportion of pixels in each of the 40 EG maps that are in the top 1% of values for that map, and averaged those proportions across conditions and subjects. We chose contrast and eccentricity values for the experiment that minimized this average proportion, resulting in a choice of contrast = 16% and eccentricity = 12°.

Subjects completed 100 trials of each of the 40 conditions (5 Reward Conditions × 8 Target Locations), for a total of 4,000 trials. The trials were split across four sessions on separate days with 25 trials per condition, randomly intermixed within each session.

The ideal-observer model

The ideal-observer model is adapted from that of Najemnik and Geisler (2005). In our adaptation, fully described in the Supplement, we modify the model to reflect the differential payoffs for correct target localizations. Consider a search task in which the precise form of the target is known to the observer and no eye movements are made. The ideal observer proceeds by means of a template match (Green & Swets, 1966), i.e., cross correlation of the retinal image with a representation of the expected target. Given a template response at each potential target location, i, the ideal observer computes the posterior probability of the target occurring at each location by Bayes' rule (Coombs, Dawes, & Tversky, 1970). In our case (see Supplement for derivation), this simplifies to

$$p(i,\mathbf{w}_1) = \frac{p(i)\exp\left[d'^2_{i,1} w_{i,1}\right]}{\sum_{j=1}^{n} p(j)\exp\left[d'^2_{j,1} w_{j,1}\right]}, \quad (5)$$

where n is the number of potential target locations, $p(i)$ is the prior probability of the target occurring at position i, and $\mathbf{w}_1 = (w_{1,1}, \cdots, w_{n,1})$ is the vector of noisy template responses from each potential target location collected during the the first fixation (F_1, the central fixation), each with corresponding detectability value $d'_{i,1}$ based on the visibility map described earlier. In our experiment, $n = 8$, and $p(i) = 1/8$, and a reward V_i is awarded for correctly detecting the target at each position i. The ideal observer selects the target position, I, with maximal expected gain:

$$I = \underset{i}{\operatorname{argmax}} \left(p(i|\mathbf{w_1}) V_i\right). \quad (6)$$

Now suppose that the target is visible long enough for one eye movement to be made. The ideal observer selects a second eye position, F_2^{opt}, that maximizes expected gain, taking into account the expected probability correct for each possible target location:

$$F_2^{opt} = \underset{F_2}{\operatorname{argmax}} \left(\sum_{i=1}^{n} p(c|i,F_2,\mathbf{w_1}) p(i|\mathbf{w_1}) V_i\right), \quad (7)$$

where $p(c|i, F_2, \mathbf{w_1})$ is the probability of being correct having chosen position i, following a saccade to location F_2, and given the template responses $\mathbf{w_1}$ from the first fixation. The derivation of F_2^{opt}, which

effectively requires a look ahead to what might happen after making the saccade, is given in the Supplement.

Following a saccade to position F_2^{opt}, the ideal observer now measures a second set of template responses ($\mathbf{w_2}$). It computes updated posterior probabilities

$$p(i|\mathbf{w}_1,F_2^{opt},\mathbf{w}_2) = \frac{p(i)\exp\left[d_{i,1}'^2 w_{i,1} + d_{i,2}'^2 w_{i,2}\right]}{\sum_{j=1}^{n} p(j)\exp\left[d_{j,1}'^2 w_{j,1} + d_{j,2}'^2 w_{j,2}\right]}, \quad (8)$$

where the values of $d'_{i,2}$ are based on the visibility map centered on the eye position after the second saccade. Finally, the ideal observer selects the location, I, for which expected gain is maximized:

$$I = \underset{i}{\operatorname{argmax}} \left(p(i|\mathbf{w_1},F_2^{opt},\mathbf{w_2})\, V_i\right). \quad (9)$$

For the ideal-observer results shown below, an ideal observer was simulated corresponding to each human observer (i.e., based on that observer's visibility map). Ideal-observer performance was computed for the same 40 conditions used in our experiments (5 Reward Conditions × 8 Target Locations), and 10 times as many trials were simulated compared to the human results (i.e., 1,000 trials/condition).

Results

Human-observer saccade endpoints

Figure 5 shows saccade endpoints for each subject across the five reward conditions in the main experiment. For each plot, the target was located at the top position. The human observers tended to make long saccades (mean across subjects and conditions = 9.94°, SD = 2.6°) to regions near potential target locations. The highest density of saccades is found near the potential target positions with the highest rewards and the actual target location (suggesting that both rewards and target information are being factored into the choice of saccade endpoint, Eckstein, Beutter, & Stone, 2001; Findlay, 1997).

We quantified the effect of the location of the target and highest reward on each subject's distribution of saccade endpoints as follows. For each actual target location, we have five spatial distributions of saccade locations (one for each reward condition). We summarized the similarity of these distributions by computing pairwise correlations. To do this, we approximated each spatial distribution by determining the number of saccades in each of a 17 × 17 grid of bins (each bin is 2° × 2°). We computed the correlation coefficient r_{ij} between the 289 bin counts for reward condition i and the corresponding bin counts for condition j. We computed the average $\bar{r}$ of the correlation coefficients corresponding to the 10 distinct pairs of reward conditions (ij).

We hypothesize that this mean correlation coefficient is low, i.e., the five spatial distributions are dissimilar due to the effect of reward condition on saccade endpoint. For this, we need a comparison distribution of mean correlation coefficients corresponding to the null hypothesis: The mean correlations expected by chance if reward location had no effect on choice of saccade endpoint. To estimate a null distribution, we generated new collections of five distributions by randomly permuting the reward-condition labels on the saccades, separately for each spatial bin. For each such randomized-labels collection of five distributions, we computed a mean correlation $\bar{r}_{perm}$ across distribution pairs as above. We repeated this procedure 1,000 times to generate a distribution of $\bar{r}_{perm}$ values for simulated datasets that shared the pooled spatial distribution of saccades of our dataset, but no effect of reward conditions. The mean correlation coefficients from the actual data ($\bar{r}$) were always lower than the lowest mean correlation coefficient from the permuted datasets. To derive a p value, we calculated the mean and SD of the $\bar{r}_{perm}$ values, and calculated a p value assuming the $\bar{r}_{perm}$ values were normally distributed. All $\bar{r}$ values are significant ($p < 0.001$), i.e., reward conditions had a significant effect on the choice of saccade endpoint.

Ideal-observer saccade endpoints

The ideal observer tended to make shorter saccades (mean across subjects and conditions = 7.94°, SD = 2.58°) than the human observers. (Note that each ideal observer is based on a visibility map, and thus there is one such ideal observer per human observer in our study.) Most of the ideal observers' saccade endpoints were near the target position with the highest reward or the actual target location (Figure 6). The ideal observers' saccade endpoints were not as diffusely distributed as the human observers'. Fewer saccades were made to target positions far from the positions with the highest reward and that containing the target, as compared to the human observers.

Comparing human- and ideal-observer saccade distributions

First we compare human and ideal observers' saccade magnitudes. The ideal observers' saccade magnitudes in the equal-rewards condition were consistently lower than those in the conditions with

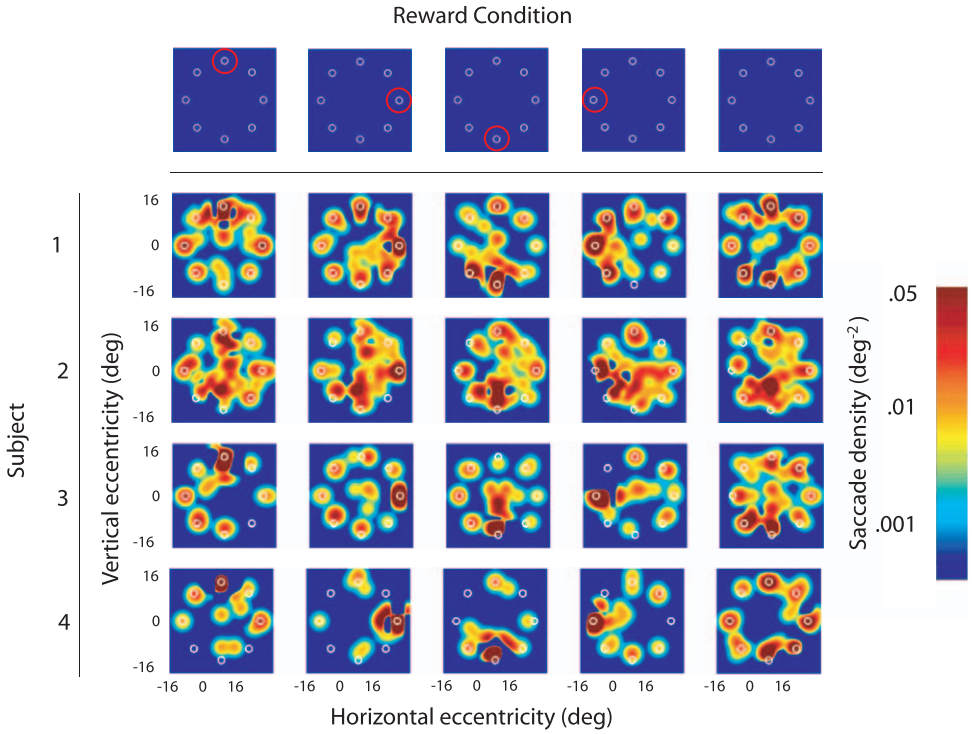

Figure 5. Human-observer saccade endpoint density maps in the main experiment. Plots are shown for all subjects and reward conditions. In all plots, the target was located at the top position. The location of the highest rewarded position is indicated by the red circles in the top row. The endpoint distributions were smoothed using a kernel density estimate (Silverman, 1986) with Gaussian radial basis functions ($SD = 1.5°$).

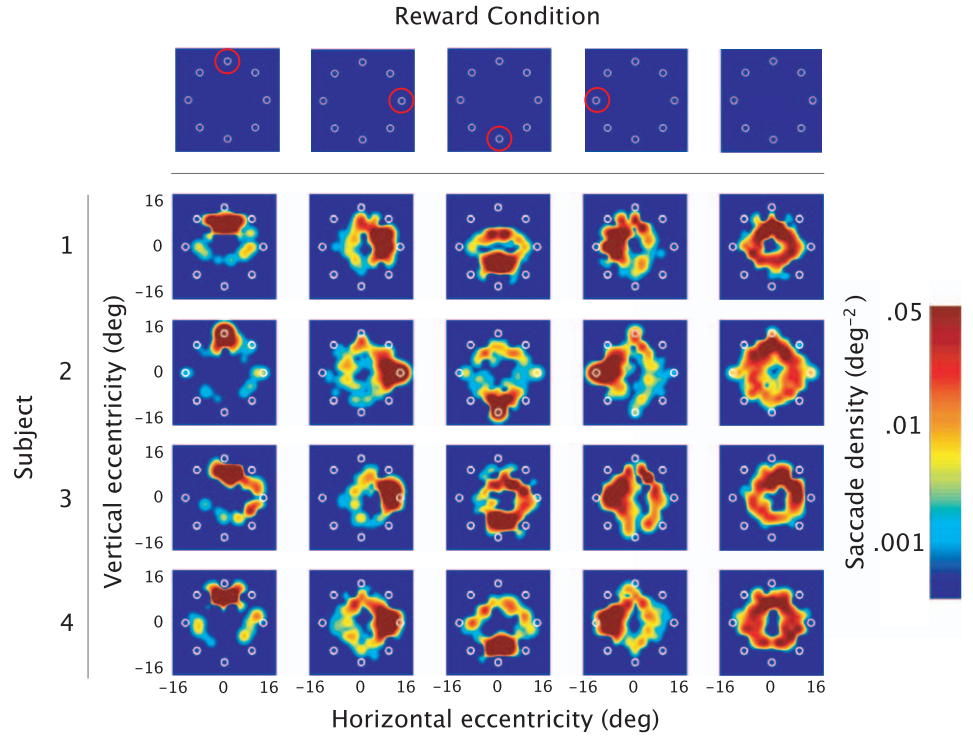

Figure 6. Ideal-observer saccade endpoint density maps. In all plots, the target was located at the top position. Other details as in Figure 5.

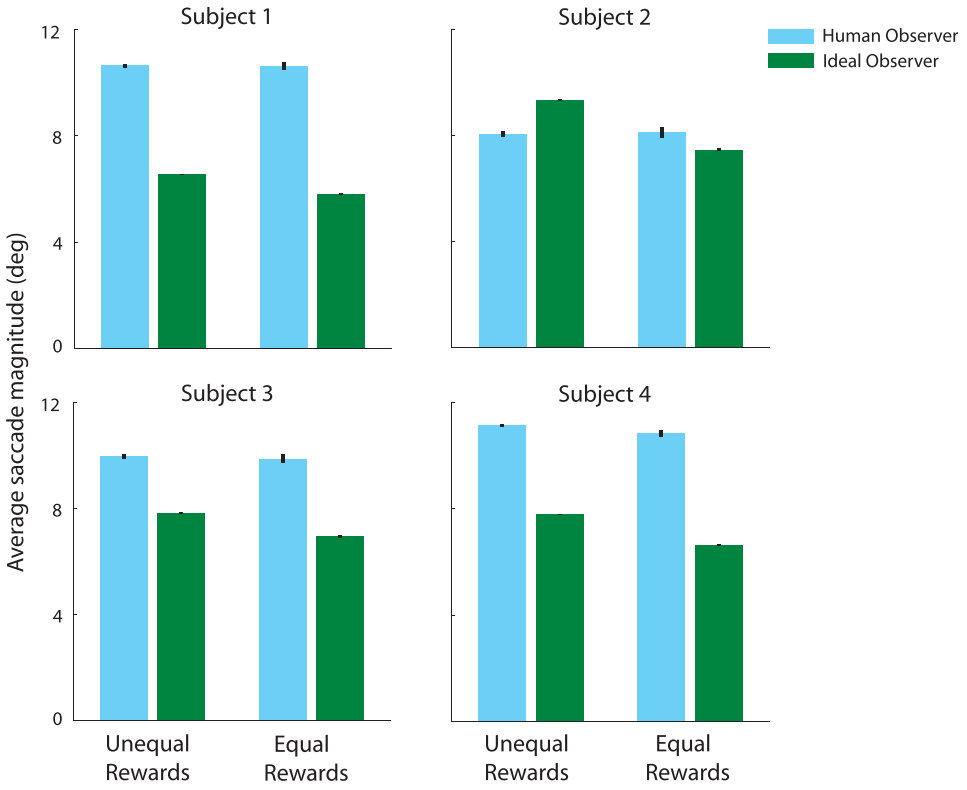

Figure 7. Mean saccade magnitude in degrees in the unequal-reward conditions (Reward Conditions 1–4) and the equal-rewards condition for human and ideal observers. Error bars are two *SE*s above and below the mean. All human and corresponding ideal-observer saccade magnitudes differ significantly ($p < 0.001$).

unequal rewards and so we compare mean magnitudes for human and ideal observers in the unequal- and equal-rewards conditions separately (Figure 7). Two-sample t tests indicate that human and ideal-observer saccade magnitudes differ significantly (all eight ps $<$ 0.001, two tailed) for every subject and both unequal- and equal-rewards conditions. In seven out of eight comparisons, the ideal observer makes shorter saccades.

Next, we compare the spatial distributions of human and ideal-observer saccade endpoints. We know that human saccades are noisy (the actual saccade endpoint varies even if the intended endpoint is fixed). Thus, to make a fair comparison, we should try to simulate the distribution of endpoints the ideal observer would make if its execution of saccades were equally variable. Van Beers (2007) provides estimates of saccade variability as a function of the distance and direction to the saccade target. According to van Beers, saccade endpoint variability increases with the length, r, of the saccade. Thus we define saccade endpoint variance, σ^2, as

$$\sigma^2(r) = a_1 r^2 + a_2. \quad (10)$$

Endpoint variance is larger along the direction of the saccade, smallest perpendicular to it, and depends on direction, θ. In the direction of the saccade, variance is lowest along the horizontal meridian and lower for upward than downward saccades. Perpendicular to the saccade, variance is lowest along the horizontal and vertical meridians and highest at the oblique angles. We model these effects, following van Beers, by setting

$$\sigma_r(r,\theta) = \sigma(r)\Big(1 + a_3\sin(\theta + a_4) + a_5\sin(2\theta + a_6)\Big)$$
$$\sigma_t(r,\theta) = a_7\sigma(r)\Big(1 + a_8\sin(4\theta + a_9)\Big), \quad (11)$$

where σ_r and σ_t are the radial and transverse standard deviations of saccade endpoint, respectively. The parameters a_i were adjusted to fit the across-subjects average data reported by van Beers (2007) leading to the variability maps and example error ellipses shown in Figure 8.

We computed the predicted distribution of saccades of the ideal observer by effectively adding variability to the ideal observer's saccades with parameters based on Equation 11. That is, in each of the 40 conditions we had a large sample of saccades made by the ideal observer. We replaced each such saccade with an elliptical Gaussian centered on the saccade endpoint, with standard deviations determined by Equation 11. These Gaussians were summed over all simulated saccades in that condition and the sum was normalized to unit volume. The resulting probability distribution

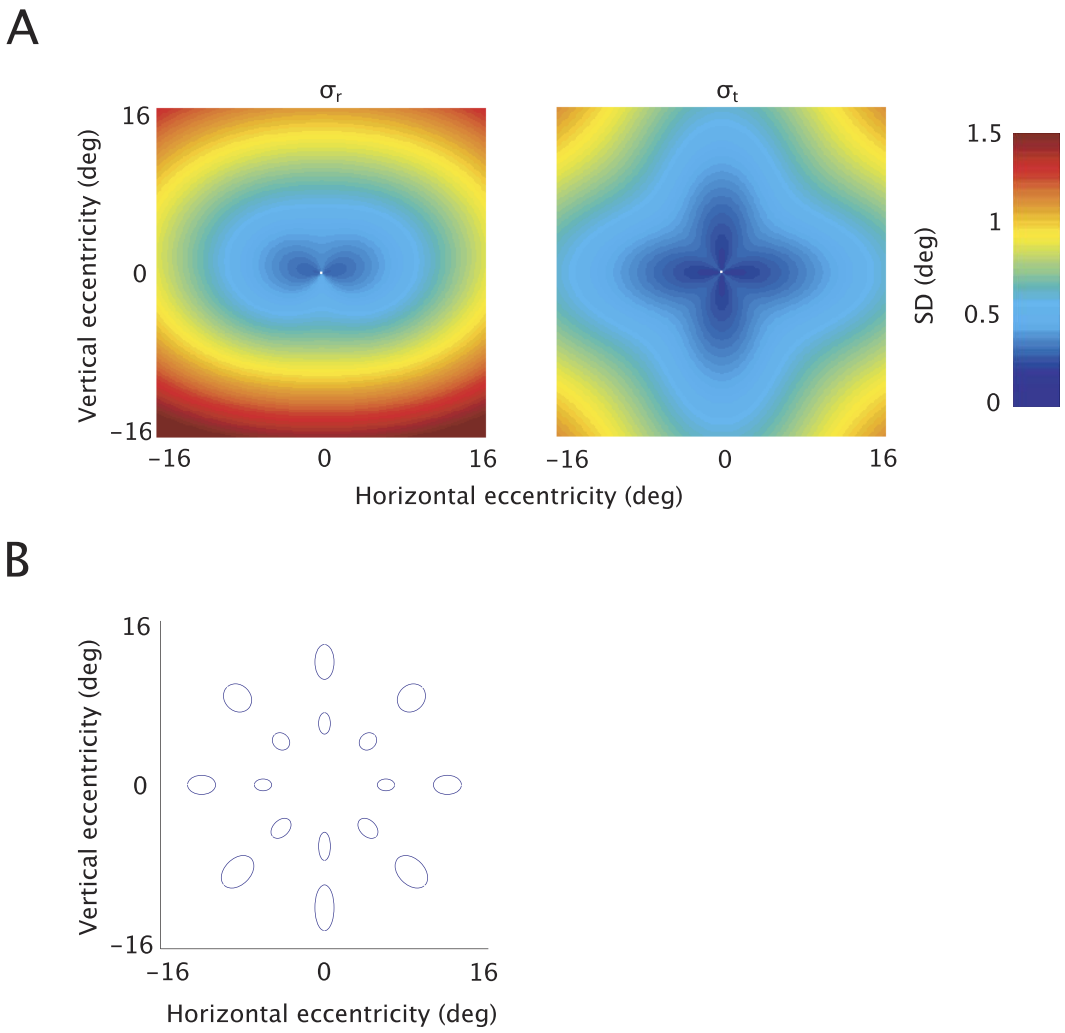

Figure 8. (A) Saccade endpoint standard deviation in the direction of the saccade (σ_r) and perpendicular to the saccade (σ_t) as a function of saccade magnitude in degrees. (B) Example error ellipses (two *SD*s) at 6° and 12° of retinal eccentricity.

was our estimate of the distribution of saccades a human observer would produce if saccade endpoints were chosen optimally.

Having determined an expected distribution of saccade endpoints for the ideal observer (with typical variability of human observers), we can compare that distribution to the measured distribution of our human observers' saccade endpoints. We use a variant of the Cramér-von Mises test for goodness of fit (Darling, 1957). This test is for goodness of fit of univariate data to a distribution and uses as a test statistic the squared error between the theoretical cumulative distribution function $F_1(x)$ and the empirical distribution $F_2(x)$:

$$\omega^2 = \int \Big(F_1(x) - F_2(x)\Big)^2 \mathrm{d}F_1(x). \tag{12}$$

Syrjala (1996) derived a bivariate analog to the above test for measuring the difference between spatially distributed populations. Each spatial array is converted into a two-dimensional histogram with K total bins. The test statistic is

$$\Psi = \sum_{k=1}^{K} \Big(\Gamma_1(x_k,y_k) - \Gamma_2(x_k,y_k)\Big)^2, \tag{13}$$

where

$$\Gamma_i(x_k,y_k) = \sum_{x \le x_k, y \le y_k} \gamma_i(x,y), \tag{14}$$

(x_k, y_k) are the horizontal and vertical coordinates of the k^{th} bin, respectively, and the estimated bin probabilities are $\gamma_i(x, y)$. The test statistic Ψ is not invariant with respect to the point in the spatial array chosen as the origin. To remove this dependency, Ψ is computed starting from each of the four corners of the array, and the resulting four values of Ψ are averaged. We computed the γ_i values using 2° × 2° bins.

We generated 1,000 random samples of 100 saccade endpoints sampled from the ideal-observer histogram and computed Ψ for each sample (comparing the

sample to the full ideal-observer histogram). The p value for the human observer's Ψ is the probability of a sample from the bootstrapped distribution having that value of Ψ or greater. There is a significant difference between human and ideal-observer saccade endpoint distributions in all conditions (all ps < 0.01).

The effect of visibility-map measurement error

We have found that the magnitude and overall spatial distribution of the human observers' saccade endpoints differ significantly from that of the ideal observer. However, the performance of the ideal observer depends on the visibility maps that we measured for each subject. We now consider the degree to which error in the measurement of the visibility maps affects the comparison of human and ideal-observer performance.

We calculated the visibility map measurement error by resampling the staircase data from the preliminary experiment at each of the 25 stimulus locations (1,000 iterations per location). The result is a distribution of the number of correct responses at each sampled contrast at each location. We calculated the 0.025 and 0.975 quantiles of the number of correct responses at each contrast at each location. Using these number-correct quantiles (and the subjects' actual total number of trials at each contrast), we derived "quantile maps." The Q_{LOW} quantile map is derived by fitting the eight-parameter psychometric function, $p(r, \theta)$ (Equations 1–3), assuming β to be constant across locations, to the 0.0275 quantile values. The Q_{HIGH} map is derived by fitting the 0.975 quantile values. The quantile maps for each subject are shown in Figure 9.

We simulated ideal observers that perform the task using each subject's quantile maps. The saccade magnitudes and spatial distribution of saccades that result represent saccades based on the upper and lower bounds on performance given each subject's visibility map measurement error. The saccade density maps for each subject's high and low quantile ideal observers are shown in Figure 10.

The lower values of d' in the peripheral regions of the Q_{LOW} maps result in longer saccades (mean = 10.36°, $SD = 1.83°$) made in the direction of the highest rewarded position and actual target location. Higher peripheral values of d' in the Q_{HIGH} maps result in shorter saccades (mean across subjects = 4.79°, $SD =$ 1.68°) made similarly into regions near the highest rewarded position and actual target location. The human observer's saccade magnitudes (mean = 9.94°, $SD = 2.6°$) lie between the values for the low- and high-quantile-map simulations.

Figure 11 shows the comparison of each human observer's saccade magnitudes with those of ideal observers using the Q_{LOW} and Q_{HIGH} visibility maps. All subjects' average saccade magnitudes in the unequal-rewards conditions are significantly less than those of the low-quantile ideal observer. This suggests that their higher saccade magnitudes (as shown in Figure 7) can be attributed to error in the visibility map measurement. All subjects' saccade magnitudes in the equal-rewards condition are greater than those for either low or high quantile simulations suggesting that this result is not attributable to error in the visibility maps.

The overall spatial distribution of saccade endpoints for the high- and low-quantile ideal observers are no more similar to those of the human observer than than they are to those of the best-estimate ideal observers as shown in Figure 5. The human observers have a higher density of saccades in regions far from the highest rewarded position or target location than either of the high- or low-quantile ideal observers. We conclude that this difference cannot be attributed to error in the visibility map measurements.

Human and ideal-observer target responses

We now ask whether human observers' suboptimal choice of saccade endpoint led to poorer performance in the search task itself. We calculated the proportion of correctly detected targets for each target position and reward condition, for both human and ideal observers (Figure 12). The pattern of performance across reward conditions is consistent for all subjects. For the unequal-rewards conditions, human performance is close to that of the ideal observer at the high-reward and adjacent locations, and generally worse at the other locations. In the equal-rewards condition, human and ideal performance are similar across target locations and the ideal observers' proportion correct is greater than the human observers'. We compared human observers' proportion correct with that of the ideal observer with a two-proportion z test. We did this by averaging the data across subjects and unequal-rewards conditions (by pooling target locations that were in identical angular positions relative to the position of the highest reward). All differences are significant ($p < 0.001$).

Are observers' suboptimal choices of saccade endpoint related to their subsequent choice of target location? To answer this question, we divided the stimulus array into eight angular and eight radial regions. The angles and radii marking the center of each region are shown in Figure 13A. The saccade endpoint data were pooled across the five reward conditions for each of the eight target positions. We would like to know whether the location of the observers' saccade endpoints relative to the target location had an effect on performance. Thus, we rotated the array and endpoints in each target

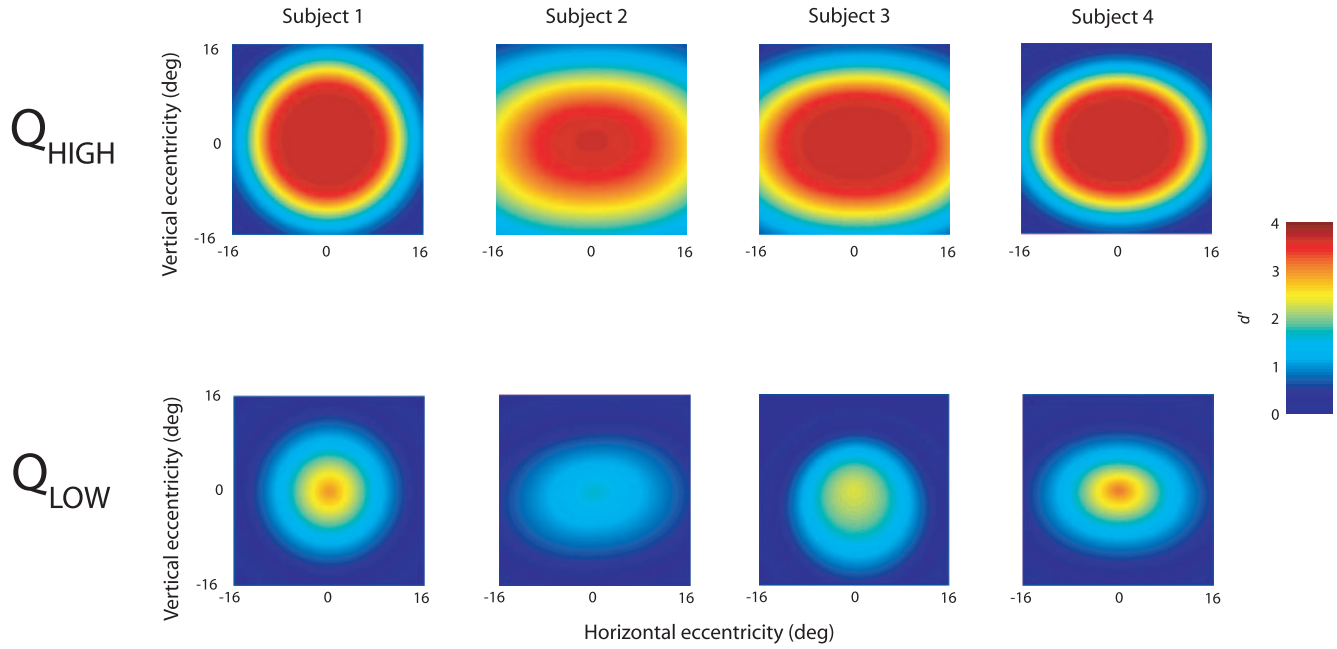

Figure 9. Visibility maps (d' as a function of retinal location for Michelson contrast = 16%) derived from the 0.0275 (Q_{LOW}) and 0.975 (Q_{HIGH}) quantiles of the resampled data from the preliminary experiment (see text).

location condition so that the target was located at 0° and pooled the endpoints across conditions. The data were then pooled across subjects and we calculated the proportion of correctly detected targets for all trials in which the saccade endpoint landed in each region. The results are shown in Figure 13B. Performance is best when saccades are made in the direction of the target or into adjacent regions and declines for saccades made to more distant regions. Thus, the choice of saccade location affects subsequent target-detection performance. However, for any given saccade direction, performance does not differ substantially as a function of saccade magnitude. This suggests that the difference in saccade magnitude we observed between human and ideal observers is not likely to have resulted in a significant effect on detection performance.

Human efficiency for target detection

In a task involving explicit rewards, the bottom line for performance is whether the human observer's strategy was costly. Thus, we now analyze human efficiency, i.e., the ratio of rewards gained by the human observer to those gained by the ideal observer. Efficiency, E, was calculated for each subject as follows:

$$E = \frac{\overline{G_H}}{\overline{G_I}}, \tag{15}$$

i.e., the ratio of the average gain per trial for the human (H) and ideal (I) observers. Efficiency for each subject is shown in Figure 14A. The standard error of each subject's mean total efficiency was derived by bootstrapping. The z tests show all total efficiencies to be significantly less than one ($p < 0.001$). Note, however, that total efficiency is quite high, with three out of four subjects earning above 75% of the expected gain of the ideal observer.

Although we find the total efficiency to be high, this result is dependent on the reward structure of our task. For example, a reward structure in which the highest reward is 5 times the lowest rather than 50 times the lowest would result in a lower total efficiency for the same choice of saccade endpoints. Thus, in order to get a measure of efficiency that is independent of the specific reward structure of the task, we would like to compare human efficiency to that of a searcher that utilizes a decidedly suboptimal saccade strategy with the same reward structure. To this end, we simulated, using each subject's visibility map, a searcher that randomly selects an endpoint on each trial (all potential saccade endpoints within 16° of the central fixation point had an equal probability of being selected) and is otherwise identical to the ideal observer.

We calculate the relative efficiency, E_{rel}, of the human observers' saccade choice as the increase in gain of the humans over the random searcher, relative to the corresponding increase made by the ideal observer:

$$E_{rel} = \frac{\overline{G_H} - \overline{G_R}}{\overline{G_I} - \overline{G_R}}. \tag{16}$$

We must consider that the observers may have low relative efficiency due not only to a suboptimal

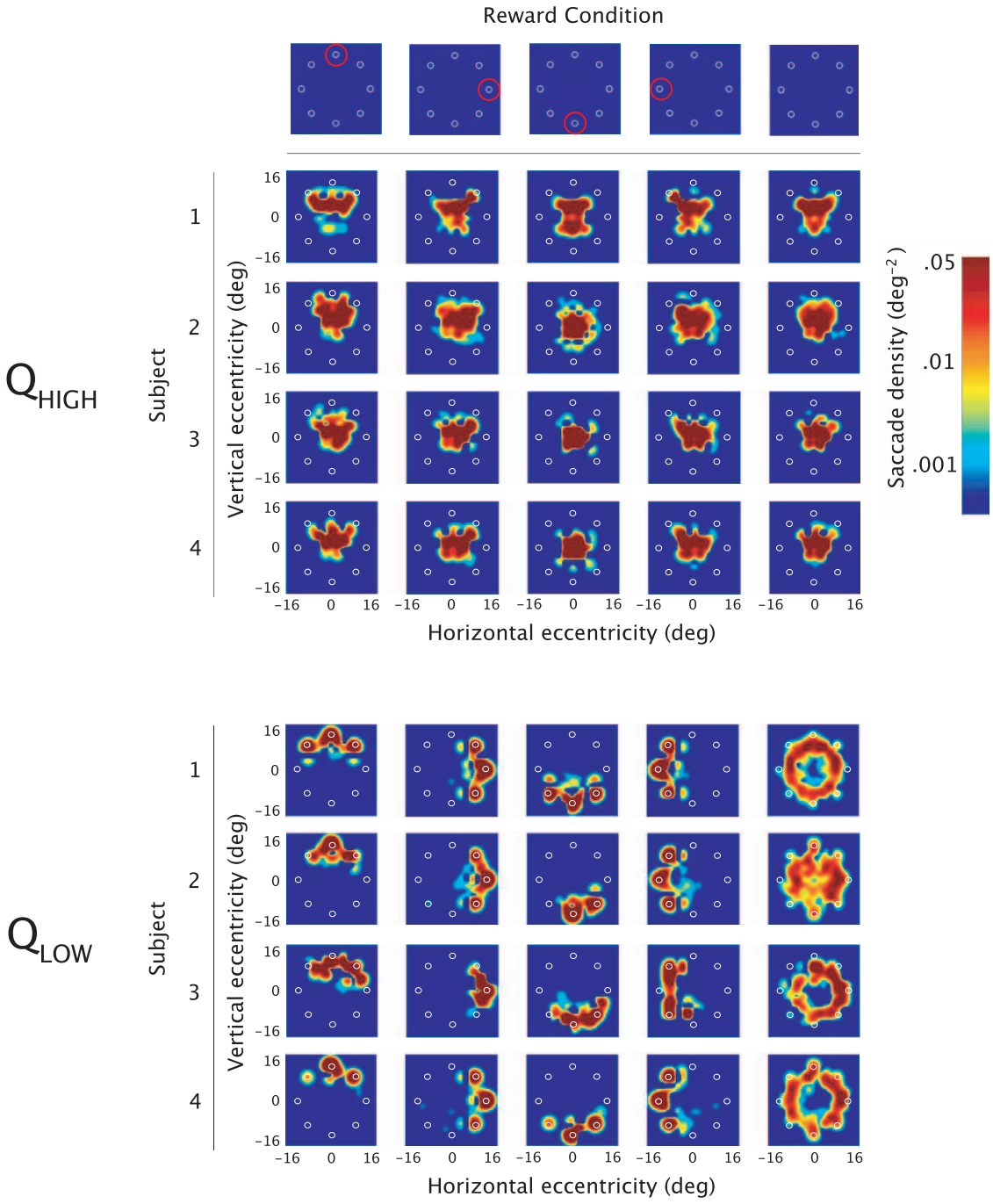

Figure 10. Saccade endpoint density maps for ideal observers using the Q_{LOW} and Q_{HIGH} visibility maps shown in Figure 9. In all plots, the target was located at the top position. Other details as in Figures 5 and 6.

choice of saccade endpoint, but also to a failure to optimally integrate information across the first and second glances. Thus, we also simulated an ideal integrator that, like the ideal observer, uses the subject's visibility map. On each trial, it generates a template response at the initial fixation, then saccades to the human observer's chosen endpoint and gets a subsequent template response from that position. It then chooses a target location in the same manner as the ideal observer. We calculated E_{rel} for the ideal integrator by substituting its average gain per trial for that of the human observer in the above equation. By comparing the ideal integrator's relative efficiency with that of the respective human observer, we can get some idea of the relative contributions of saccade endpoint and information integration on efficiency. The results are shown in Figure 14B.

Values of E_{rel} less than one indicate suboptimal behavior. E_{rel} is significantly less than one for all subjects ($p < 0.001$). Negative values of E_{rel} indicate

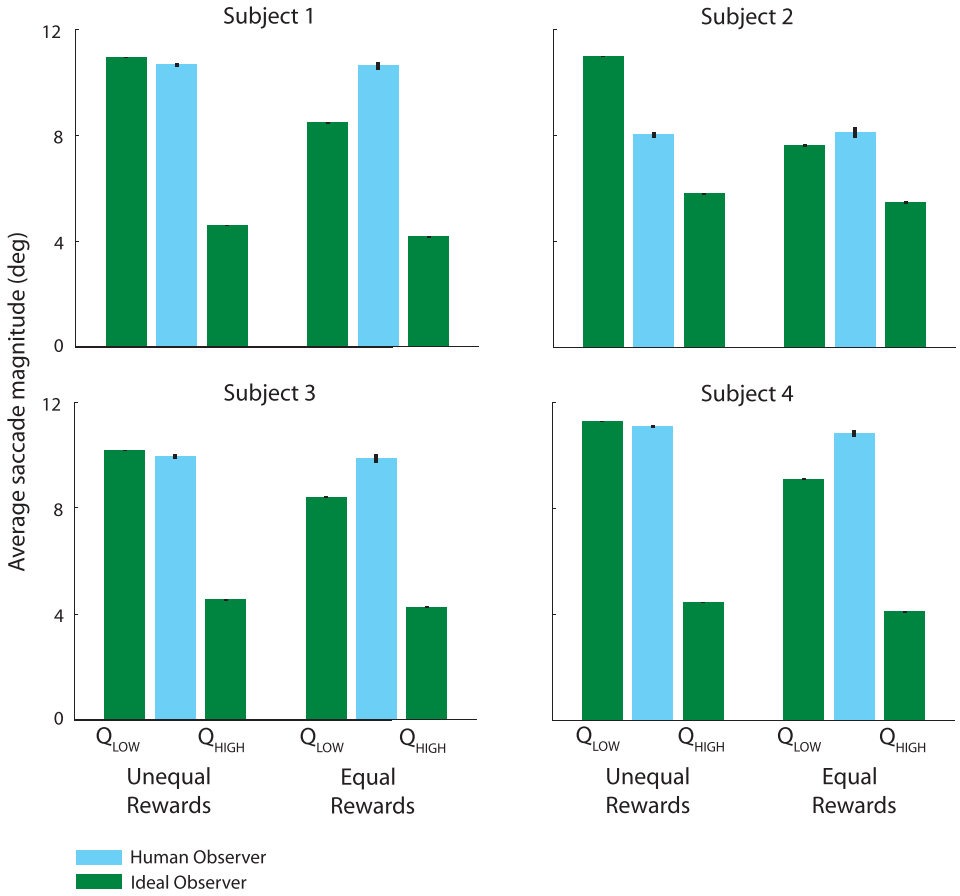

Figure 11. Mean saccade magnitude in degrees in the unequal-reward conditions (Reward Conditions 1–4) and the equal-rewards condition for the human observers and ideal observers utilizing the Q_{LOW} and Q_{HIGH} visibility maps. Error bars are two *SE*s above and below the mean. All human and corresponding ideal-observer saccade magnitudes differ significantly ($p < 0.001$).

that the human observer's choice of saccade endpoint resulted in gain lower than that of the random searcher. The z tests, with the SE derived by bootstrapping, show E_{rel} for Subjects 1 and 2 to be significantly less than zero ($p < 0.01$). Subject 3 and 4's E_{rel} values are not significantly different from zero.

These results suggest that suboptimal choice of saccade endpoint has a substantial cost to the human observers independent of the reward structure of the task. That the efficiency of Subjects 1 and 2 is substantially worse than that of the random searcher is likely due to suboptimal integration of information across saccades. This conclusion is borne out by comparing Subject 1 and 2's E_{rel} with that of the corresponding ideal integrator. The ideal integrator's E_{rel} is higher for both subjects indicating that Subjects 1 and 2's negative E_{rel} values are due, at least in part, to suboptimal integration. That the ideal integrator's E_{rel} is lower than zero for all subjects suggests that the human observers' strategy for selecting an endpoint is worse than that of the random searcher's in terms of its effect on efficiency. We conclude that subjects' suboptimal choice of saccade endpoint, in combination with suboptimal integration across saccades, resulted in a significant loss of rewards.

Finally, we consider the effect of visibility map measurement error on efficiency. As described above, error in the measurement of the visibility map parameters tending toward the lower quantiles of the parameter distributions results in an increase in d' in the periphery and, consequently, higher probability correct for target detection on the part of the ideal observer. The efficiency of the human observer, in this case, would be as low or lower than that shown in Figure 14. On the other hand, error in the measurement of the visibility map parameters tending toward the higher quantiles of the parameter distributions results in lower probability correct on the part of the ideal observer. Note that performance of the human observers, as shown in Figure 12, is relatively close to that of the ideal observers, particularly when the target appears at the highest rewarded, or adjacent, locations. A decrease in performance on the part of the ideal observer quickly leads to the situation in which the human observers' performance exceeds that of the respective ideal

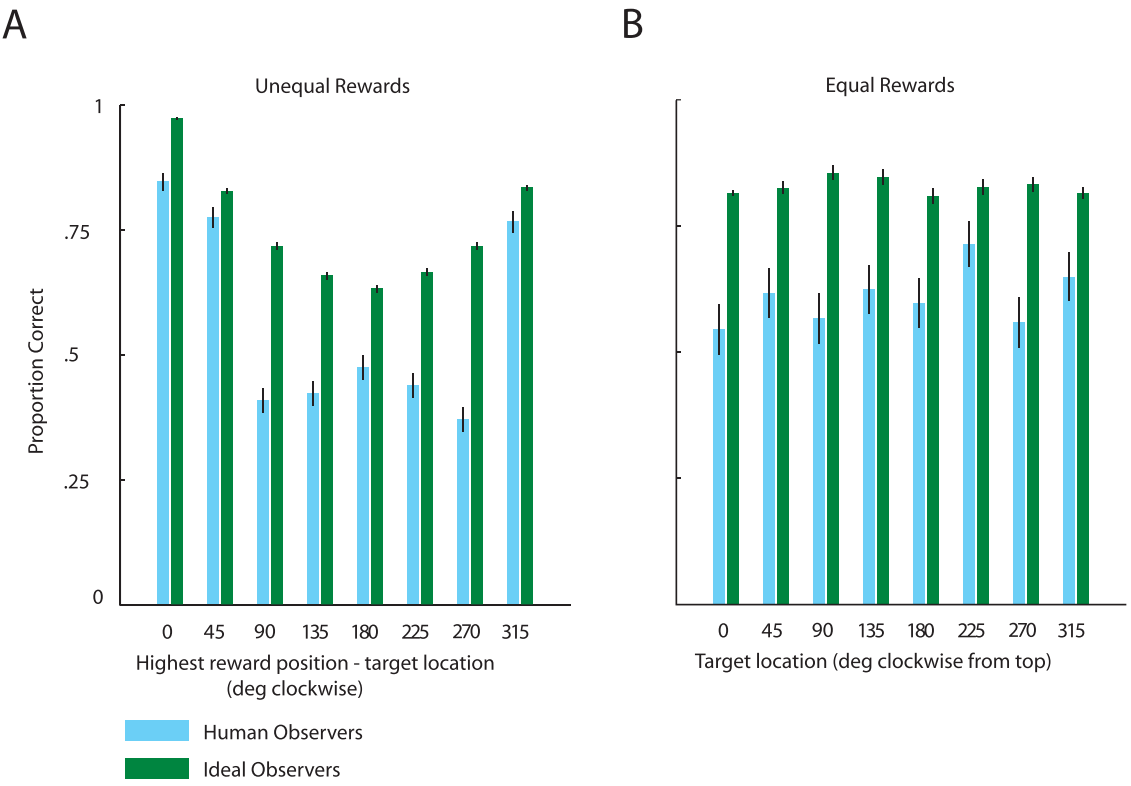

Figure 12. (A) Proportion correct for human and ideal observers averaged across subjects and across unequal-reward conditions, where locations were pooled by their position relative to the highest rewarded position in each condition. Error bars are ±2 *SE*s. All differences between human and ideal observers are significant ($p < 0.001$). (B) Proportion correct averaged across the equal-reward conditions. All other details as in (A).

observer. This indeed results in higher efficiency for the human observer. However, performance of the human observer in excess of that of the ideal observer is indicative, not of high efficiency, but of either (a) error in the visibility map, such that it does not accurately represent the human observer's underlying response to the stimuli, or (b) error in the cost function that is optimized by the ideal observer. We address the possibility that the human observers may employ a cost function entirely different from that of the ideal observer in the Discussion. We conclude that the visibility maps, as measured, are more accurate than those that may be derived from a higher quantile of the parameter distribution and that efficiency, as measured, is not substantially affected by visibility map measurement error.

Discussion

We conducted a visual search task in which observers made a single saccade prior to deciding where the search target was located. We asked whether observers choose the saccade endpoint that maximizes expected gain when the value of correctly detecting the target varies across potential target locations. The observers' chosen saccade endpoints and target choices were compared to those of an ideal observer that maximizes monetary gain given the human observer's ability to detect the target as a function of retinal location.

Patterns of human and ideal-observer saccades are qualitatively similar. Both tend to saccade into regions near the target position with the highest reward and nearest the actual target location. However, the human observers' choices of saccade endpoint differed significantly from those of the ideal observers in that they had a higher density of saccades far from the highest rewarded and actual target positions.

The human observers' ability to correctly detect the target approached that of the ideal observer when the target was located at the position with the highest reward or at adjacent positions and tended to be lower when the target was located at more distant positions. The human observers' suboptimal choice of saccade endpoint, i.e., making saccades to regions far from the highest rewarded position, resulted in a lower proportion of correctly detected targets.

In spite of the cost to the observer of a suboptimal choice of saccade endpoint in terms of being able to correctly detect the target, the cost in terms of earned

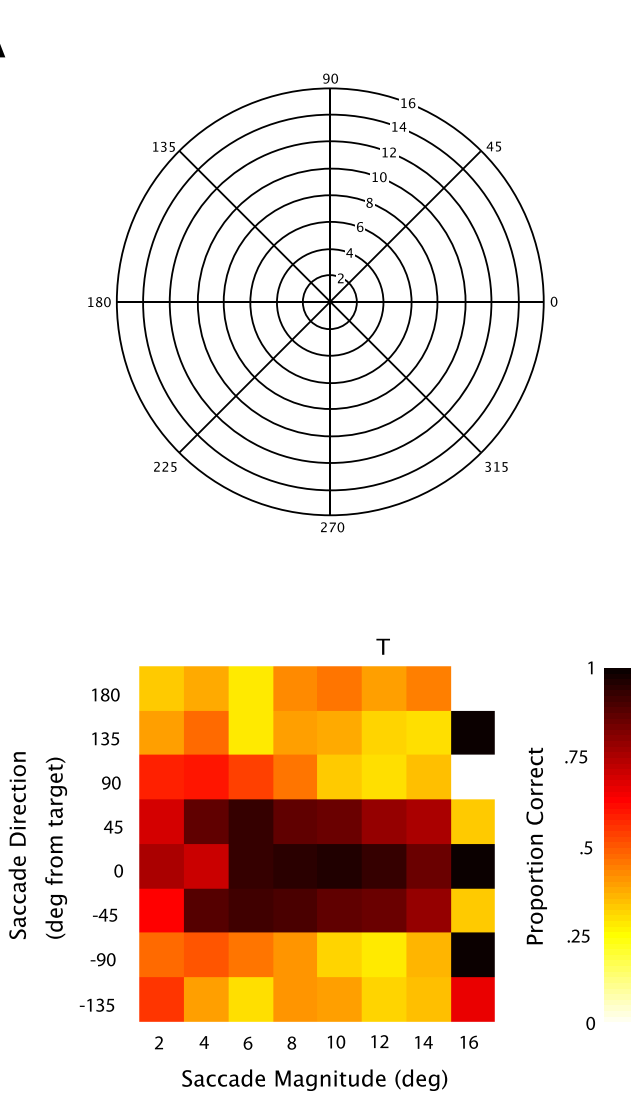

Figure 13. (A) The angular (degree) and radial (degrees of visual angle) centers of the saccade-endpoint pooling regions. (B) Proportion correct target detection, across subjects, for trials on which the saccade landed in each pooling region. Saccade magnitude is in degrees of visual angle. In the top panel, "T" indicates the target eccentricity at 12°. Positive angular values of the saccade direction are counterclockwise from the target. White space indicates that the pooling region contains no data.

rewards was modest. The overall monetary gain of three out four subjects was above 75% of that earned by the ideal observer. However, efficiency computed in this way depends on the reward structure of our task. To determine the degree to which observers' efficiency depended on their choice of saccade endpoint independent of reward structure, we compared human observers' efficiency to that of a simulated searcher that randomly selects a saccade endpoint on every trial. We found that human observers' efficiency was equal to or lower than that of the random searcher. This result, however, assumes that the human observer optimally integrates the template responses from the initial fixation and subsequent saccade endpoint. To account for the possible influence of suboptimal integration on efficiency, we simulated an "ideal integrator" that optimally integrates the template responses generated at the human observer's initial fixation and saccade endpoint on each trial, prior to choosing a target location. The ideal integrator's relative efficiency was not better than that of the random searcher. It was greater than that of two out of four subjects suggesting that their low relative efficiency was due in part to suboptimal integration. In sum, the suboptimal choice of saccade endpoint in combination with suboptimal integration of information across saccades resulted in a substantial cost to the observers.

What factors might have caused the human observers to choose a pattern of saccade endpoints different from the ideal observer? The human observer's choice of saccade endpoint as modeled here depends on three factors: (a) a template response to the stimuli from which the posterior probability of the target occurring at each potential location is calculated, (b) an estimate of target detectability at each possible saccade endpoint, and (c) the value of detecting the target at each location. We address each factor in turn.

The observer's internal response to a stimulus is assumed, under signal detection theory, to be a random draw from a distribution with parameters that are constant for a given target contrast and retinal location. These parameters were measured in our preliminary experiment and used to model the visibility maps. However, it has been noted that the assumption of normally distributed responses to signal and noise is not necessarily correct (Maloney & Thomas, 1991). The actual underlying, unobservable distributions may take on any number of forms. If there is a discrepancy between the underlying distribution and the functional form used in our experiment, this could lead to mismodeling of the visibility maps and a misconstrual of the observers' chosen saccade endpoints as suboptimal.

Before making a saccade, the observer estimates the visibility, d', of the target at each potential saccade endpoint. The observer may under- or overestimate d' by, for example, over- or underestimating the variance of the noise, respectively, and thus mistake variability in the noise images at a nontarget locations for the signal. An overestimation of d' across the visual field could result in higher saccade magnitudes, as found with the human observers, as, in the observer's mind, the eye may travel further from potential target locations with less risk of nondetection at distant locations. We simulated a subideal observer in our task that generates template responses to the stimulus at each potential target location using the actual d's from

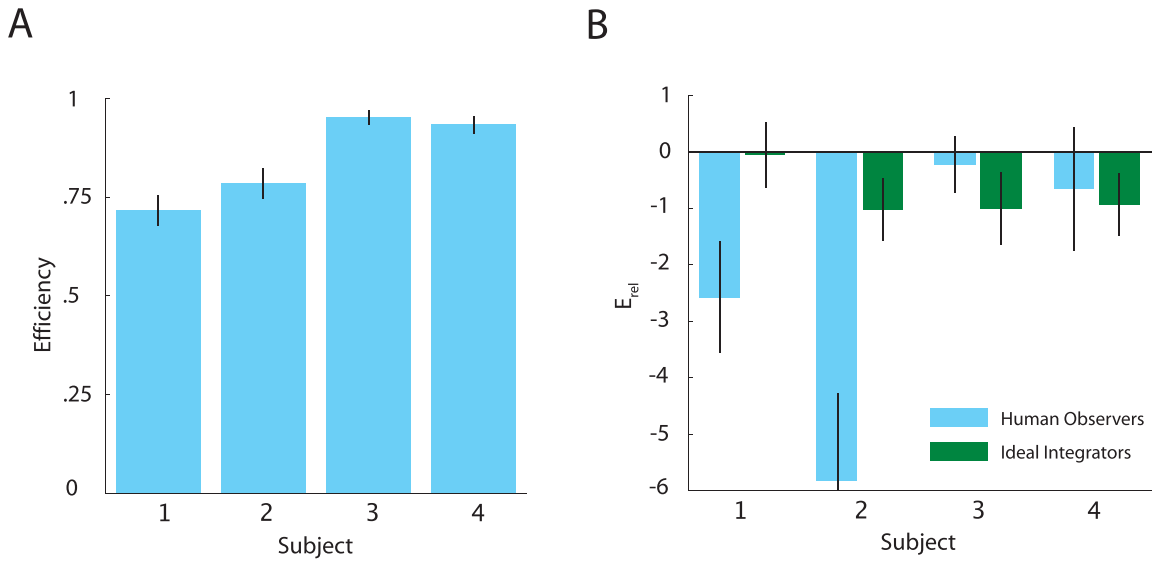

Figure 14. (A) Efficiency for each subject. Error bars are ±2 *SE*s determined by bootstrapping. (B) Relative efficiency, E_{rel}, for each human observer and corresponding ideal integrator (see text). Values less than one indicate suboptimal performance. Values less than zero indicate performance that is worse than that of a searcher that chooses saccade endpoints at random.

the respective observer's visibility map. It then overestimates d' at every location by a factor of two in the process of calculating posterior probabilities and the probability of a correct response at each potential saccade endpoint. The result, as predicted, is an increase in saccade magnitude similar to that of the human observers. However, overestimation of d' also resulted in an increase in the proportion of saccades made near to the actual target location regardless of the location of the highest reward. This is unlike the pattern we found with the human observers, who tended to make the highest density of saccades to regions near the highest rewarded position.

It is possible that observers apply a nonlinear weighting to the rewards thereby basing their selection of saccade endpoint on expected utility rather than expected gain (Fox & Poldrack, 2009; Kahneman & Tversky, 1979). The result would likely be a more diffuse distribution of saccades made to locations far from the highest rewarded position, similar to that found in the equal-rewards condition of our task. We simulated an ideal observer that under-weights potential gains by applying an exponent of 0.5 to all rewards prior to choosing a saccade endpoint. The resulting saccade distributions are more diffuse, as predicted. However, there is primarily an increase in the density of short saccades and in the density of saccades made in the direction of the actual target location. This is unlike our human observers who made a high density of long saccades to distant target locations.

We also rule out an overweighting of rewards, e.g., applying an exponent greater than one to all rewards. As the value of the overweighted reward increases, the expected gain of saccades made to all potential saccade locations is nearly equated, with slightly higher expected gain at the highest rewarded position. Saccade selection ceases to have any bearing on earned rewards. The best strategy is to simply select the highest rewarded position and ignore stimulus information. We would predict a high density of saccades made to the highest rewarded position where expected gain as a function of retinal location has a small, nominal peak. Simulations employing an ideal observer that squares all rewards (an extreme risk-seeking strategy) prior to selecting a saccade endpoint result, as predicted, in a high density of saccades made to the highest rewarded position

Another possible explanation of observers' suboptimal choice of saccade endpoint is that they adopted a strategy entirely unlike the ideal observer. The ideal observer chooses the saccade endpoint that maximizes expected gain summed across all potential target locations. Saccade magnitudes tend to be small and the endpoints tend to be in the direction of the highest rewarded position or actual target location. Human observers' saccade endpoints tend to lie closer to the potential target locations. Perhaps the human observers adopted a strategy in which they saccaded to a potential target location, I, with the highest expected gain for choosing it as the location of the target (Equation 6):

$$I = \underset{i}{\operatorname{argmax}} \left(p(i|\mathbf{w_1}) V_i \right), \tag{17}$$

and then made a saccade to that location ($F_2^{\text{human}} = I$).

In essence, this strategy involves first selecting a *consideration set* (Roberts & Lattin, 1991) of possible saccade endpoints that includes only the potential target locations. A target location is then chosen given

the first exposure to it at the initial point of fixation and the choice is confirmed by making a saccade to the chosen location. The strategy is risky in that if the initial choice turns out to be wrong, the saccade, and second exposure to the target, will have yielded little useful information about the target's actual location. The misplaced saccade will have placed most of the potential target locations far from fixation. The second exposure to the target will likely produce a low internal response. Consequently, the posterior probabilities of target occurrence at all locations will be nearly equal and the expected gain of any subsequent choice of target location will be relatively low. This is a problem that the present ideal observer inherently avoids by choosing saccades that maximize expected gain summed across all potential target locations. However, it may be that the timing constraints of our task make it impossible for a human observer to perform the calculation of the optimal saccade endpoint, thus making this risky, suboptimal strategy more feasible than the ideal observer's. Given limited time to gather information and make a decision, the best strategy may be to choose a saccade endpoint that maximizes expected gain at the position where it is already highest rather than maximizing gain across all locations. The current paradigm does not offer a fair comparison between the risky strategy described above and that of the current ideal observer as the former only saccades to potential target locations and the latter is free to saccade to any location. Thus, we leave it to future research to compare the two strategies in terms of their relative effectiveness in harvesting gains under various timing constraints.

To conclude, we address potential improvements to our paradigm. First, we have not addressed the possible effects of attention. It has been shown that attaching a reward to a stimulus enhances its saliency (Hickey, Chelazzi, & Theeuwes, 2010; Theeuwes & Belopolsky, 2012) and that attention enhances the discriminability and perceived contrast of a target prior to a saccade being made to it (Rolfs & Carrasco, 2012; White, Rolfs, & Carrasco, 2013). In measuring our visibility maps, there were no rewards associated with the target stimuli and subjects maintained fixation throughout a trial. Thus, d' as a function of eccentricity in the main experiment (in which there were rewards and saccades were made) may have differed from that measured in the preliminary experiment. The paradigm could be improved by making the task used to measure the visibility maps more similar to the main experiment by employing rewards and allowing saccades.

An additional concern is that, in the main experiment, we present the rewards associated with each target location prior to initiation of the trial. This gives the observer ample time to preplan a saccade to the highest rewarded location. If the saccade is preplanned, this may decrease the influence of the subsequently presented target stimulus on the choice of saccade endpoint. A paradigm with multiple saccades may control for this possibility.

The comparison of human and ideal observers is made more meaningful when the cost incurred for suboptimal performance is substantial. Although we made an effort to maximize the expected gain of an optimal saccade endpoint, the total efficiency of subjects in our task, in spite of their suboptimal performance, was high. The paradigm could be improved by increasing the cost of a suboptimal saccade. Expected gain as a function of eccentricity in our task depends on the rewards and the observer's visibility map (which itself depends on stimulus contrast). The expected gain surface could be made steeper, that is, the peak of the surface could be made more distinct, by artificially altering the observer's visibility map. By, for example, adding noise to the display that increases with eccentricity, visibility could be made to decrease more abruptly with eccentricity with a concomitant decrease in expected gain.

Keywords: visual search, ideal observer, saccade

Acknowledgments

This work was supported by NIH Grant EY08266. We would like to thank Miguel Eckstein and an anonymous reviewer for comments that helped us improve this paper substantially.

Commercial relationships: none.
Corresponding author: Michael S. Landy.
Email: landy@nyu.edu.
Address: Department of Psychology, New York University, New York, NY, USA.

References

Bisley, J., & Goldberg, M. (2010). Attention, intention, and priority in the parietal lobe. *Annual Review of Neuroscience, 33,* 1–21.

Carrasco, M., Talgar, C. P., & Cameron, E. L. (2001). Characterizing visual performance fields: Effects of transient covert attention, spatial frequency, eccentricity, task and set size. *Spatial Vision, 15,* 61–75.

Coombs, C. H., Dawes, R. M., & Tversky, A. (1970). *Mathematical psychology: An elementary introduction*. New York, NY: Prentice Hall.

Cornelissen, F. W., Peters, E. M., & Palmer, J. (2002).

The eyelink toolbox: Eye tracking with matlab and the psychophysics toolbox. *Behavior Research Methods: Instruments and Computers, 34,* 613–617.

Darling, D. A. (1957). The Kolmogorov-Smirnov, Cramér-von Mises tests. *The Annals of Mathematical Statistics, 28,* 823–838.

Eckstein, M., Beutter, B., & Stone, L. (2001). Quantifying the performance limits of human saccadic targeting during visual search. *Perception, 30,* 1389–1401.

Efron, B., & Tibshirani, R. (1993). *An introduction to the bootstrap*. New York, NY: Chapman and Hall.

Findlay, J. (1997). Saccade target selection during visual search. *Vision Research, 37,* 617–631.

Fox, C., & Poldrack, R. (2009). Prospect theory and the brain. In P. Glimcher, C. Camerer, E. Fehr, & R. Poldrack (Eds.), *Neuroeconomics: Decision making and the brain* (pp. 145–173). New York, NY: Elsevier.

Geisler, W., Perry, J., & Najemnik, J. (2006). Visual search: The role of peripheral information measured using gaze-contingent displays. *Journal of Vision, 6*(9):1, 858–873, http://www.journalofvision.org/content/6/9/1, doi:10.1167/6.9.1. [PubMed] [Article]

Green, D., & Swets, J. (1966). *Signal detection theory and psychophysics*. New York, NY: Kreiger Publishing Co.

Herrnstein, R. (1970). On the law of effect. *Journal of the Experimental Analysis of Behavior*, *13*, 243–266.

Hickey, C., Chelazzi, L., & Theeuwes, J. (2010). Reward changes salience in human vision via the anterior cingulate. *The Journal of Neuroscience, 30,* 1096–1103.

Kahneman, D., & Tversky, A. (1979). Prospect theory: An analysis of decision under risk. *Econometrica, 4,* 263–291.

Liston, D., & Stone, L. (2008). Effects of prior information and reward on oculomotor and perceptual choices. *The Journal of Neuroscience, 28,* 13866–13875.

Liu, T., Heeger, D. J., & Carrasco, M. (2006). Neural correlates of the visual vertical meridian asymmetry. *Journal of Vision, 6*(11):12, 1294–1306. http://www.journalofvision.org/content/6/11/12, doi:10.1167/6.11.12. [PubMed] [Article]

Maloney, L. T., & Thomas, E. A. C. (1991). Distributional assumptions and observed conservatism in the theory of signal detectability. *Journal of Mathematical Psychology, 35,* 443–470.

Michel, M., & Geisler, W. S. (2011). Intrinsic position uncertainty explains detection and localization performance in peripheral vision. *Journal of Vision, 11*(1):18, 1–18, http://www.journalofvision.org/content/11/1/18, doi:10.1167/11.1.18.

Najemnik, J., & Geisler, W. (2005). Optimal eye movement strategies in visual search. *Nature, 434,* 387–391.

Navalpakkam, V., Koch, C., Rangel, A., & Perona, P. (2010). Optimal reward harvesting in complex perceptual environments. *Proceedings of the National Academy of Sciences, USA, 107,* 5232–5237.

Previc, F. H. (1990). Functional specialization of the upper and lower visual fields in humans: Its ecological origins and neurophysiological implications. *Behavioral and Brain Sciences, 13,* 519–575.

Renninger, L. W., Verghese, P., & Coughlan, J. (2007). Where to look next? Eye movements reduce local uncertainty. *Journal of Vision, 7*(3):6, 1–17, , http://www.journalofvision.org/content/7/3/6, doi:10.1167/7.3.6. [PubMed] [Article]

Roberts, J., & Lattin, J. (1991). Development and testing of a model of consideration set composition. *Journal of Marketing Research, 28,* 429–440.

Rolfs, M., & Carrasco, M. (2012). Rapid simultaneous enhancement of visual sensitivity and perceived contrast during saccade preparation. *The Journal of Neuroscience, 32,* 13744–13752.

Silverman, B. W. (1986). *Density estimation for statistics and data analysis*. London, UK: Chapman and Hall.

Sugrue, L., Corrado, G., & Newsome, W. (2004). Matching behavior and the representation of value in the parietal cortex. *Science, 304,* 1782–1787.

Syrjala, S. E. (1996). A statistical test for the difference between the spatial distributions of two populations. *Ecology, 77,* 75–80.

Theeuwes, J., & Belopolsky, A. (2012). Reward grabs the eye: Oculomotor capture by rewarding stimuli. *Vision Research, 74,* 80–85.

Treutwein, B. (1995). Adaptive psychophysical procedures. *Vision Research, 35,* 2503–2522.

van Beers, R. J. (2007). The sources of variability in saccadic eye movements. *The Journal of Neuroscience, 27,* 8757–8770.

White, A., Rolfs, M., & Carrasco, M. (2013). Adaptive deployment of spatial and feature-based attention before saccades. *Vision Research*, *85,* 26–35.

Wickens, T. D. (2002). *Elementary signal detection theory*. New York: Oxford University Press.